Investigation on Electrochemical Jet Machining of High Volume Fraction SiC$_p$/Al Composite

Zhuang Liu[!], Changshui Gao[!,], Yi Qiu, Chao Guo*

College of Mechanical and Electrical Engineering, Nanjing University of Aeronautics and Astronautics, 29 Yudao Street, Nanjing 210016, China
[!]These authors contributed equally to this work and should be considered co-first authors
[*]E-mail: meecsgao@nuaa.edu.cn

SiC particles reinforced aluminum matrix composites (SiC$_p$/Al) is a class of materials with a wide potential for application in aerospace and electronic packaging. High volume fraction reinforcement SiC$_p$/Al is very difficult to machine by conventional methods. This research investigated electrochemical jet machining (ECJM) of 65%-SiC$_p$/Al composite with absence of and presence of abrasive assistance. The machining capability and material removal mechanism have been analyzed for the jet process. The results show that the material removal mechanism involves corrosion of matrix followed by SiC particles pullout. The presence of abrasives in the ECJM process can remove oxide layer generated at aluminum surface and results in relatively higher machining rate than pure ECJM. The craters due to SiC particles pullout and SiC protrusion due to corrosion of matrix significantly affect roughness of the machined surface.

1. INTRODUCTION

Particle reinforced metal matrix composites (MMCs) exhibit less density and higher specific properties, e.g. strength and stiffness etc., that are hard to obtain from a single material [1]. Common matrix metals include aluminum, titanium, magnesium, copper and various alloys of these materials. The reinforcement is generally a brittle ceramic material and typical examples of that are silicon carbide (SiC) and boron carbide [2]. As a typical MMCs, SiC particles reinforced aluminum matrix composites (SiC$_p$/Al) has been increasingly used in aerospace, electronic packaging, precision instrumentation and automotive industry, as stated by Huang et al. [3]. The investigation of Müller and Monaghan [4] shows that machining SiC$_p$/Al using conventional processes such as milling, turning, drilling etc., generally

results in excessive tool wear and worse surface finish because the SiC particles have significant higher hardness than metal matrix. Thus non-conventional techniques have also been applied to these materials. However, Pramanik [5] found that machining of high content reinforcement of this composite (e.g. 65%-SiC$_p$/Al) using non-conventional techniques still meet much difficulties.

As explained by Saxena et al. [6], electrochemical jet machining (ECJM) technology enables removing metals and forming complex surficial geometries in micro-scale dimensions through concentrating a DC current in an electrolyte jet ejected from a nozzle. Generally, high working voltage and high conductivity electrolytes are used in this process in order to achieve high current density and subsequently high material removal rate. Compared to electrochemical machining (ECM), the ECJM can restrict the current in the jet and obtain a better machining localization. The ECJM is capable of fabricating micro-structured surfaces and three-dimensional geometries by changing the machining gap distance and choosing proper current setting. For example, Hackert-Oschätzchen et al. [7] reported ECJM of micro grooves with approximate 100-200 μm in width at stainless steel using a Ø100μm jet and a 30wt% NaNO$_3$ electrolyte. A simulation model for predicting workpiece deformation based on current density calculation was also introduced in that paper. Bisterov et al. [8] presented ECJM of complex surface texture using a Ø500 μm jet and a 2.3M-NaNO$_3$ electrolyte, supported by a developed specific CAM software. It was found the surface texture can be repeatedly controlled in a range from 0.04 to 0.5 μm. Mitchell-Smith et al. [9] investigated ECJM of micro-grooves with various cross-sectional profiles using several specifically designed nozzle tips. These nozzle tips, shaped as different geometries, can alter the localized distance between nozzle and workpiece at discrete points, and consequently change the current density.

Compared to machining of metals, very few literatures reported ECJM of SiC$_p$/Al composites. Lehnert et al. [10] experimentally investigated ECJM of 5%- and 10%-SiC$_p$/Al composites using pH-neutral aqueous electrolytes of sodium bromide, sodium chloride and sodium nitrate. They found that the deepest point erosions were generated using NaCl electrolyte, and the point erosion generated by using NaNO$_3$ have the lowest depth. Theoretically, the ECJM machinability of SiC$_p$/Al composites is highly related with the content of the SiC reinforcement, because the anodic dissolution can remove aluminum matrix but cannot corrode the non-conductive SiC particles. Therefore, the ECJM of high volume fraction SiC$_p$/Al composites is still a great challenge and has not been explored yet.

The abrasive assisted electrochemical jet micro-machining (AECJM) is a hybrid process removing metals by anodic dissolution and erosion simultaneously [11]. In AECJM process, a neutral electrolyte mixed with abrasives is employed as working liquid to form a micro jet exiting from a nozzle with a relatively high velocity to impinge and remove target material. The presence of abrasives in ECJM can improve material removal rate and obtain better surface roughness. Similar to ECJM, the AECJM can be applied to fabricate micro features such as micro holes and micro grooves at various metal surface. For example, Liu et al. [12] reported AECJM of micro-channels with complex patterns at stainless steel using a Ø300 μm jet, a 3-4MPa jet pressure and a sodium nitrate electrolyte mixed with Al$_2$O$_3$ abrasives. Che et al. [13] investigated surface machining of Ti-6Al-4V alloy using AECJM and found that the flowing abrasives can effectively remove the TiO$_2$ oxide film generated at metal surface. Theoretically, the AECJM can be used to machine SiC$_p$/Al composites because it is hypothesized that the corrosion due to electrochemical reaction can remove aluminum matrix surround reinforcement, meanwhile the

SiC reinforcement can be pulled out of workpiece through impingement of liquid jet and abrasives. The presence of abrasives in the working liquid can provide a high frequency pulsed impact force on the SiC particle, and subsequently shorten the lifetime of the interface between matrix and reinforcement. However, the AECJM of SiC_p/Al composite remains unexplored. The objective of this paper is to investigate and compare the capability of machining high volume fraction SiC_p/Al composite applying ECJM and AECJM.

2. EXPERIMENTAL DESIGN

2.1 Experimental setup

The experimental apparatus is composed of a vertical X-Y stage, a nozzle head, a diaphragm metering pump, a working liquid tank, a pulsation damper, a DC power supply and a current logger, as illustrated in Fig. 1. The nozzle head was made by stainless steel and assembled with a 300 μm diameter sapphire orifice in it. The metering pump was used to propel the working liquid (pre-mixed abrasive water, or electrolyte, or pre-mixed abrasive electrolyte) through the nozzle head to form an approximately ø300 μm jet. The gap distance between nozzle and specimen can be regulated between 0 to 20 mm to meet experimental requirement. The DC power supply, which has a output voltage up to 200 V, was used to provide a working voltage between metal nozzle and target for the experiments. The machining current can be sampled and stored by the current logger during the processes. The specimen was mounted on the X-Y stage that could move in two-dimensional direction during fixation of the specimen.
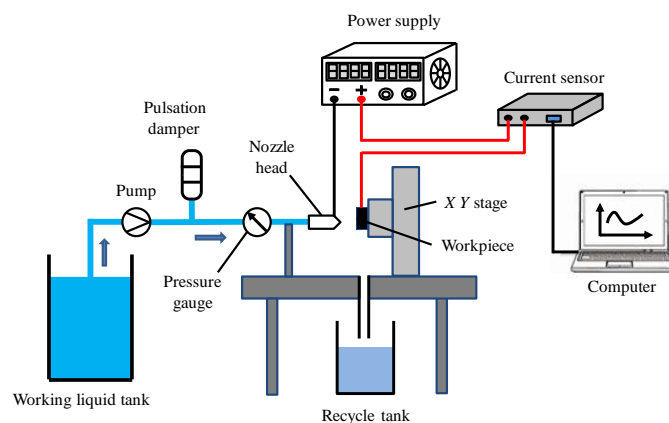

Figure 1. Schematic of experimental apparatus

2.2 Materials and experimental design

The specimens used in the experiments are 65%-SiC_p/Al plates in 5mm thickness, provided by Hunan Harvest Technology Development Company (China). The SiC reinforcements have irregular shapes and its size is between 100-120 μm. Fig.2 exhibits a microscope photo of the surface topography of the target material. Angular alumina (Al_2O_3) abrasive particles with a nominal diameter of 10 μm were added to the working liquid at room temperature for the AECJM experiments.
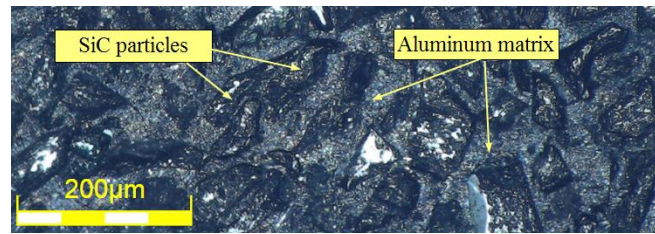
Figure 2. Surface topography of the 65%-SiC_p/Al composite

Table 1 lists process conditions for the experiments. The gap distance between target and nozzle was regulated as 2, 5 and 10 mm during the process to investigate the machining capability relevant to target distance. 15wt% $NaNO_3$ electrolyte was used as working liquid. Additionally, 1wt% Al_2O_3 abrasives were mixed into the electrolyte for the AECJM. The applied working voltage was fixed as 150V, and the machining gap was regulated as 2 and 5 mm for the AECJM and ECJM. A series of blind holes were machined under stationary jet impact at varied processing time between 1-3 minutes during the experiments. Each machining experiment was performed twice to obtain two results for subsequent measurement.

Table 1. Process conditions

Process parameters	ECJM	AECJM
Target material	65%-SiC_p/Al	65%-SiC_p/Al
SiC particle size	100-120 μm	100-120 μm
Jet diameter (mm)	0.3	0.3
Jet pressure (MPa)	4	4
Gap distance (mm)	2,5	2,5
Abrasive type & concentration	None	1wt%-Al_2O_3
Abrasive size	None	10 μm
Electrolyte type	15wt%-$NaNO_3$	15wt%-$NaNO_3$
Applied voltage (V)	150	150
Processing time (min)	1,2,3	1,2,3

2.3 Measurement

Each machined hole was measured to obtain three-dimensional topography, entry diameter, depth, cross-sectional profiles, surface roughness R_a and removed volume using an optical microscope (Olympus DSX-510). The three-dimensional topography was acquired by scanning the hole with a step size of 2 μm in two planar directions. The cross-sectional profile of that can be obtained from the scanned topography. The machining current was sampled by the current logger at a frequency of 1 Hz for each experiment. The entry diameter and depth were averaged by the measured results of X direction and Y direction separately, as illustrated in Figs. 3(a) and 3(b). The roughness R_a was measured at the center

position of the bottom using evaluation length of 800 μm and cutoff length of 250 μm, as exhibited in Fig. 3(c).
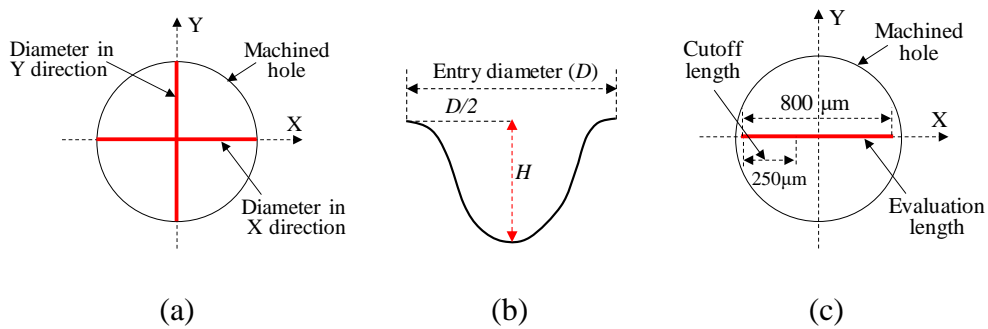

Figure 3. Measurement of machining result: (a) entry diameter, (b) depth, and (c) roughness R_a

3. RESULTS AND DISCUSSION

3.1 Machining without abrasive assistance

3.1.1 Machining results

Figs. 4 and 5 illustrate scanned photos of typical machined results due to ECJM at 2mm target distance and different processing time. Other conditions include jet pressure of 4 MPa, electrolyte of 15wt%-NaNO$_3$ and working voltage of 150V. Fig.6 shows measured cross-sectional profiles resulted from varied processing time and gap distance. According to the measured results, these machining formed geometric shapes of blind holes with entry diameter approximate ranges from 0.6 to 1.0 mm, depth ranges from 0.4 to 0.8 mm, and surface roughness R_a ranges from 10 to 16 μm. The hole entry is approximate 2-3 times bigger than the jet diameter. Similar to the ECJM of a single metal material, the removed volume increased with machining time and decreased with gap distance.
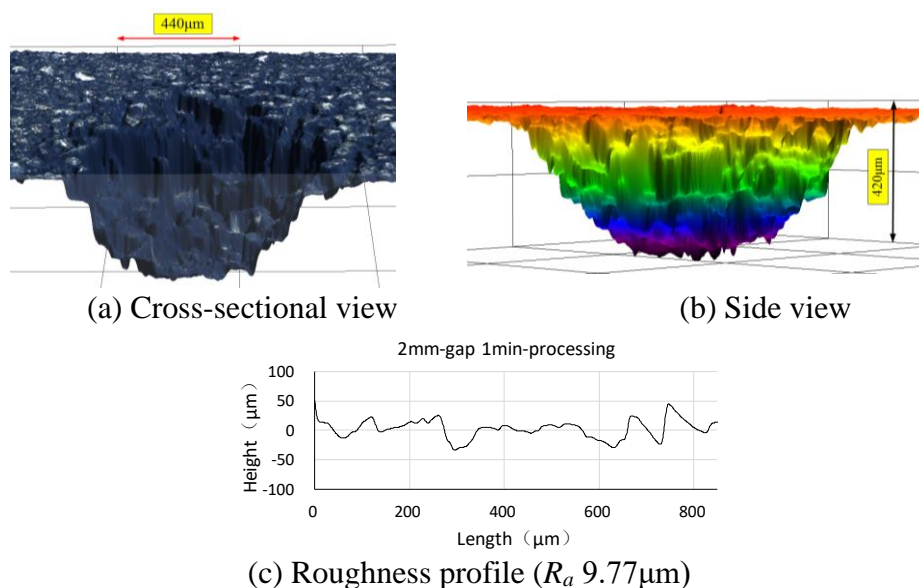

(a) Cross-sectional view   (b) Side view

(c) Roughness profile (R_a 9.77μm)

Figure 4. Machined results due to ECJM at 2mm gap distance and 1 min processing time

(a) Cross-sectional view   (b) Side view

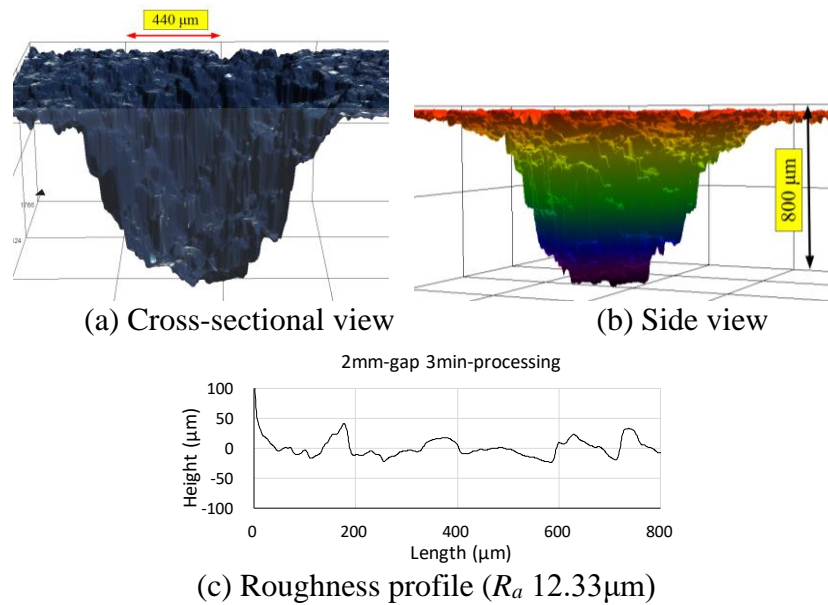(c) Roughness profile (R_a 12.33μm)

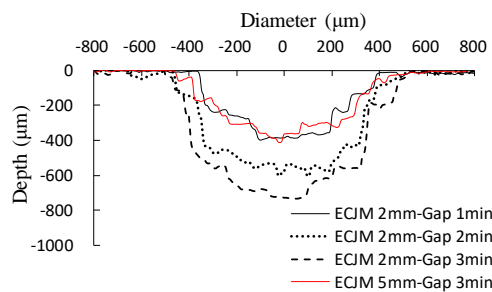**Figure 5.** Machined results due to ECJM at 2mm gap distance and 3 min processing time


Figure 6. Typical cross-sectional profiles due to ECJM at varied processing time and gap distance

3.1.2 Dissolution of aluminum matrix and pullout of SiC reinforcement

Lohrengel et al. [14] discovered that aluminum dissolves in passive state and forms cations (Al^{3+}) as products in the ECM with neutral electrolytes. Ano et al. [15] also found that the aluminum can be oxidized to Al^{3+} at anode in a corrosive environment. Therefore, the main reactions taking place at electrodes in electrochemical machining can be described as:
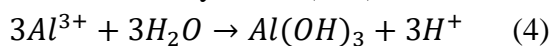
At the anode (oxidation):

$$Al \rightarrow Al^{3+} + 3e^- \qquad (2)$$
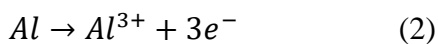
At the cathode (reduction):

$$3H_2O + 3e^- \rightarrow \frac{3}{2}H_2 + 3OH^- \qquad (3)$$
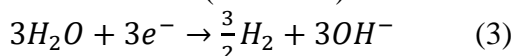
Al^{3+} ions generated by electrochemical oxidation in the process may form aluminum species, which transform finally into *Al(OH)₃*:

$$3Al^{3+} + 3H_2O \rightarrow Al(OH)_3 + 3H^+ \qquad (4)$$

In the meantime, Lohrengel et al. [14] found that there is a high possibility that an oxide film of less than 10 nm generates adjacent to the metal surface which can be continuously removed by electrolyte flow. This electrochemical step proceeds at the interface metal/oxide can be described as:

$$2Al + 3H_2O \rightarrow Al_2O_3 + 6H^+ + 6e^- \quad (5)$$
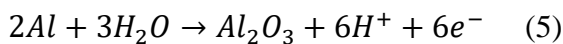
Equations (2)-(5) explain the dissolution of aluminum in a neutral electrolyte. According to Faraday's Law, the metal dissolution speed along surface normal v_c (mm/min) can be expressed as follows:

$$v_c = \eta \omega \vec{J_n} \quad (6)$$

where η denotes the current efficiency, ω (mm^3/A·min) denotes the volumetric electrochemical equivalent of the material and J_n (A/mm^2) is current density. Thus, the metal removal rate R (mm^3/min) can be expressed as:

$$R = v_c \times S_c \quad (7)$$

where S_c (mm^2) denotes the actual corrosion area.

Taking the machining of 150V voltage, 2mm gap distance and 1 min processing time as an example to estimate corrosion rate of aluminum matrix. A machining current was measured as 33 mA, that is approximate 0.33 A/mm^2 according to the corrosion area (having almost doubled diameter than impinging jet, investigated by Hackert-Oschätzchen et al. [16]) with 35% of that is aluminum and 65% of that is SiC. The ω can be adopted as 2.1 mm^3/A·min, the current efficiency η can be set as 60% according to the investigation of Haisch et al. [17]. Then the calculated removal rate of aluminum matrix should be 0.0416 mm^3/min. The measured volume loss in 1 min machining time for ECJM of 65%-SiC$_p$/Al is 0.11 mm^3, and therefore the actual removal rate of matrix is 0.0385 mm^3/min which has a 7.5% deviation compared to the theoretical calculation.

During the dissolution of aluminum matrix, the reinforcements start protruding out of the surface and the interface area between SiC particle and matrix becomes lowering. In this stage, the current distribution at the machining area is highly non-uniform. As shown in Fig. 7(a), the maximum density of electric flux lines should occur around the edges between SiC particle and matrix (Zone B). That results in higher current density along these edges than other area (Zone A), and consequently results in faster dissolution rate at these edges. This is similar to the ECM process with insulated mask, because the protruded parts of the SiC particles can be treated as an insulated film which covers approximate 65% of the machining surface. Some literatures studied and explained this phenomenon in ECM through insulated mask. For example, West et al. [18] compared simulated through-mask ECM profile of axisymmetric geometry to experimental result. They found that, for small aspect ratio of mask opening (approximate 0.1), the maximum etch rate occurs near the photoresist mask, and it moves toward the center of the metal as the etching proceeds. However, with an increase in etch depth, the current distribution becomes more uniform, and the maximum etch rate moves to the center. Baldhoff et al. [19] studied current distribution of through-mask electrochemical micro-machining and found, in the case of a low-aspect-ratio mask opening, the initial current distribution is highly non-uniform. The maxima occur along the edges between mask and metal substrate. With an increase in etch depth, then the current distribution becomes more uniform, and the maxima merge in the center. Therefore, the matrix enclosed by SiC particles can be dissolved in a relatively more uniform shape compared to ASJM machining, as demonstrated in Fig. 7(b). The continuous dissolution of matrix results in a continuous decrease of the

interface, and the reinforcement will be finally pulled out in case the bonding interface failed under continuous jet flushing, as shown in Fig. 7(c).
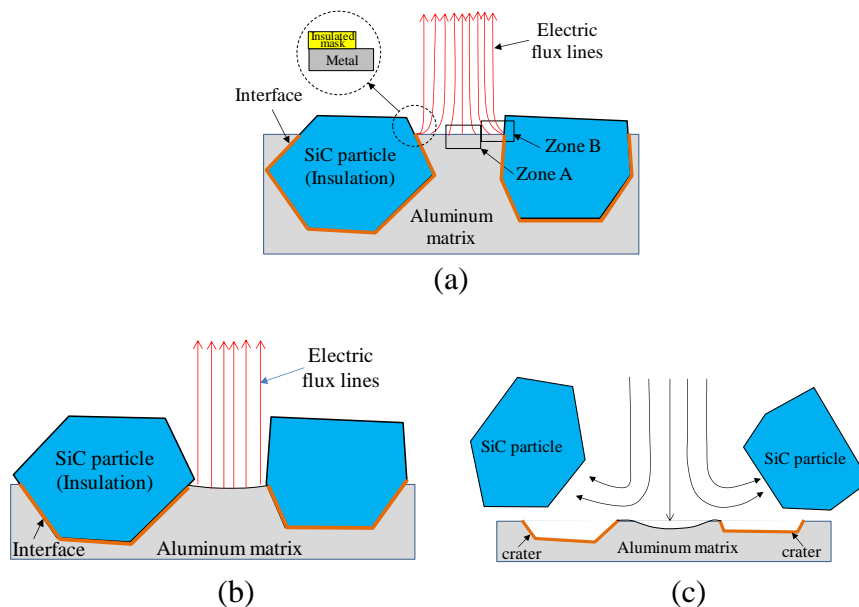

Figure 7. Removal of SiC reinforcement in ECJM: (a) hypothesized electric field distribution at matrix area, (b) reduction of interface area, and (c) SiC particles pull out due to jet flush

The pullout of SiC reinforcements result in many micro craters at the machined surface, as illustrated in Fig. 8. In the meantime, some SiC particles start protruding out of the surface because surround matrix has been dissolved due to corrosion. This will cause a relatively rough machining surface. The measured cross-sectional views, side views and roughness profiles and cross-sectional profiles (as shown in Figs.4-6) are proofs of that. Apparently, larger size SiC reinforcement or higher content of the reinforcement will lead to higher roughness of the machined surface.
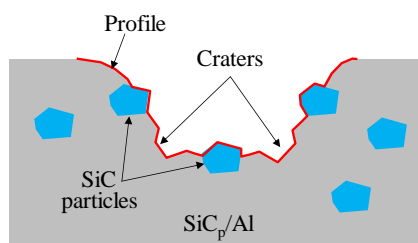

Figure 8. Schematic of machining profile

3.1.3 Machining current

Fig. 9 shows the measured machining current across the jet for conditions of 2 mm gap and 3 min processing time. The current shows a character that starts from low value and continuously increases with machining time, and fluctuates with many jumps, as shown in Fig. 9. This character is relevant to evolution of the machining hole and SiC particles pull out during the material removal.
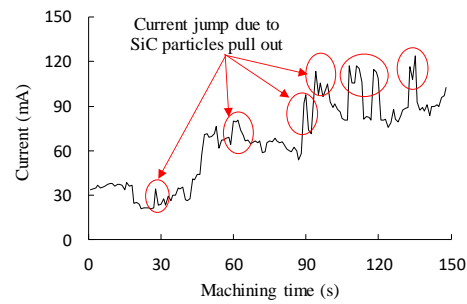
Figure 9. Measured current in the ECJM of SiC$_p$/Al at 2 mm gap and 3 min processing time.

In ECJM, the electrolyte jet flows from nozzle (cathode) to workpiece (anode) at a very high velocity and a constant gap distance. Hackert-Oschätzchen et al. [16] explained that the potential applied across nozzle and workpiece generates an electric field between them, resulting in local current density at workpiece and correspondent anodic dissolution of material. The current across the jet should be an integral of local current density at local corrosion area:

$$\begin{cases} J_n = -\kappa \left(\frac{\partial \Phi}{\partial x} e_x + \frac{\partial \Phi}{\partial y} e_y + \frac{\partial \Phi}{\partial z} e_z \right) \\ I = \int_s J_n ds \end{cases} \tag{8}$$

where J_n denotes the current density induced by potential applied between nozzle and workpiece, κ denotes the electrolyte conductivity, $\Phi(x, y, z)$ is potential of a local point at anode surface, $n(e_x, e_y, e_z)$ is the normal of a local point at anode surface, I is the current across the jet, S represents the total corrosion area at anode. The J_n normally distributes as a Gaussian distribution and the peak current density is located at the center of the jet, as explained by Mitchell-Smith et al. [9].

As discussed previously, the effect of anodic dissolution of matrix and continuous jet flushing cause the SiC reinforcement pull out from material when the interface area shrinks to relatively small. The leaving of SiC particle occurs in a very short period due to high speed jet flow, and creates a micro crater at the machining surface thereafter. Because the mean size of the SiC reinforcement is relatively large (approximate 100-120 μm), the sudden presence of a micro crater will result in a sudden increase of corrosion area, as illustrated in Fig. 10. In the meantime, the current density J_n at most local positions will not change because conditions for generating electric field do not change in that period. As a result, a sudden increase of corrosion area S will cause a sudden increase of current across the jet, as described in Eq. (8). This is consistent with the character of the actual measured current as Fig. 9. It can be seen, the machining current has many pulsed-form jumps (marked with red circles) during the whole processing time. These current jumps are highly related with the transient change of corrosion area due to one or more SiC particles pull out. It is also found in the Fig. 9 that all of these current jumps are followed by a slight current drop. This is because some new SiC reinforcements start protruding out of machining surface after matrix has been dissolved, and subsequently results in a temporary decrease of corrosion area.
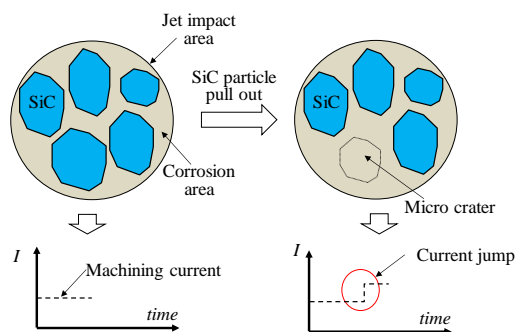
Figure 10. Hypothesized characters of machining current due to ECJM of SiC_p/Al

Fig. 9 also shows that, from the prospective of the whole processing time, the machining current increases with the time. This is relevant to the continuous increase of entry diameter during the process, resulting in an increase of corrosion area and current in total. This is consistent with the findings of Hackert-Oschätzchen et al. [16] who studied the jet shape at the anode surface and found that the current density distributed in a circular area, approximately having double diameter than jet size from the nozzle. In the meantime, the current density reaches maximum at the jet center where owns the maximum dissolution rate, and declines to zero at the boundary, as demonstrated in Fig.11. It means that the actual corrosion area at anode is initially almost in double diameter of the jet (*d*). This corrosion area will continuous increase with processing time, and subsequently results in an increase of entry diameter. In addition, for ECJM of SiC_p/Al composites, the impinging jet generates impact force along jet direction on the SiC particles at bottom, like particle-A in Fig.11. This vertical impact force will cause pressure stress at the interface between reinforcement and matrix. However, for the SiC particle on sidewall, like particle-B in Fig.11, the return flow will produce a pressured flush at side of the protruding part of the particle and generate a shear stress to the interface. Compared to pressure stress, the shear stress can break the interface in a fast way. Therefore, the SiC particles on the sidewall should be removed easier than those at bottom. This is another reason that the entry diameter was increased with processing time.
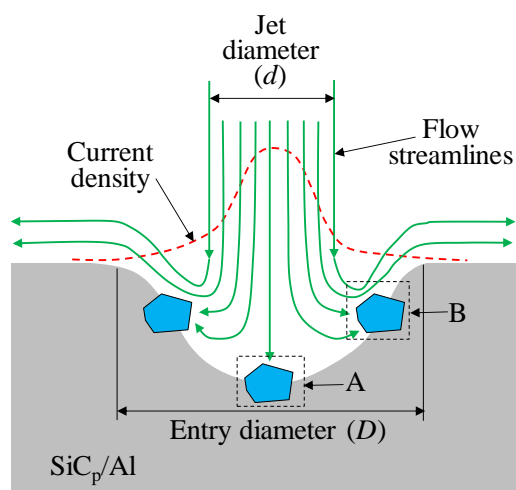

Figure 11. Hypothesized distribution of current density and flow streamlines under a whole jet area

3.2 Machining with abrasive assistance

3.3.1 Machining results

Figs. 12, 13 and 14 illustrate typical machined results due to AECJM at varied gap distance and processing time. The machining conditions of 2mm gap and 1 min processing time achieved a typical result (Fig.12) with entry diameter, depth and surface roughness of 790 μm, 322 μm and R_a 15.48μm. The conditions of 2mm gap and 3 min processing time achieved a typical result (Fig.13) of 1146 μm, 662 μm and R_a 13.35 μm. The machined results of 5 mm gap and 3 min (Fig.14) are 902 μm, 406 μm, R_a 16.27 μm, respectively.
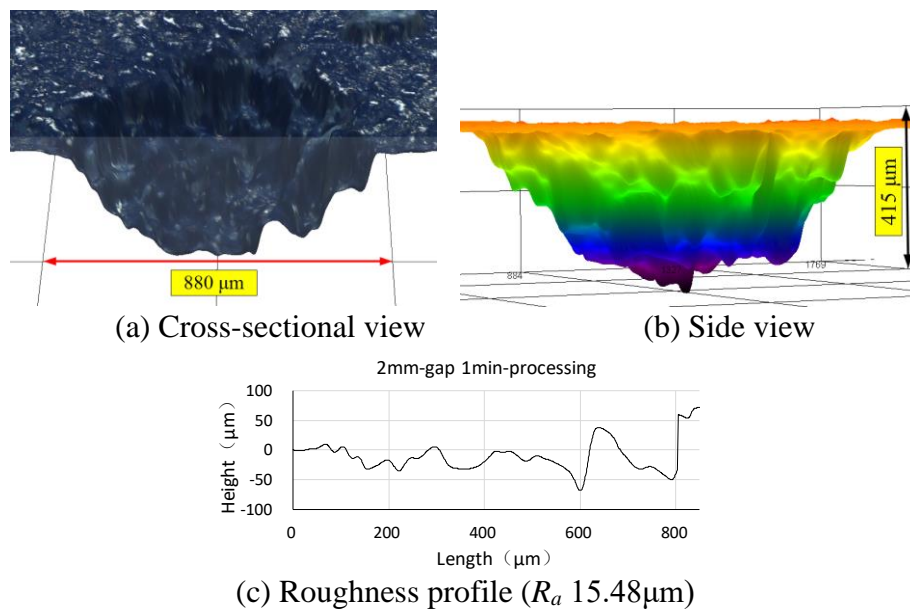

(a) Cross-sectional view   (b) Side view

(c) Roughness profile (R_a 15.48μm)

Figure 12. Machined results due to AECJM at 2mm gap and 1 min processing time

(a) Cross-sectional view   (b) 3D topography of machined area

(c) Roughness profile (R_a 13.35μm)
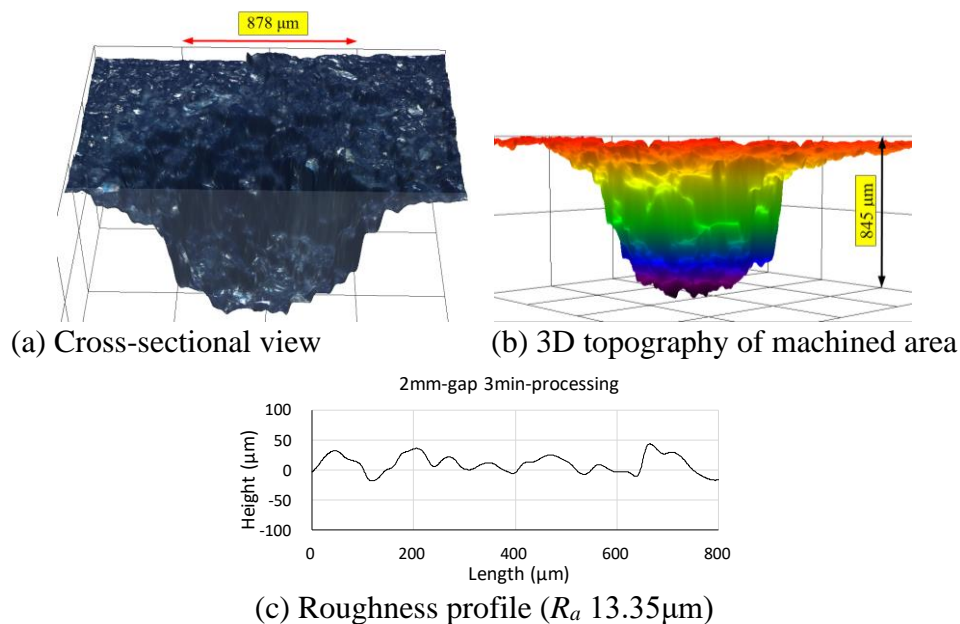
Figure 13. Machined results due to AECJM at 2 gap and 3 min processing time

(a) Cross-sectional view   (b) Side view
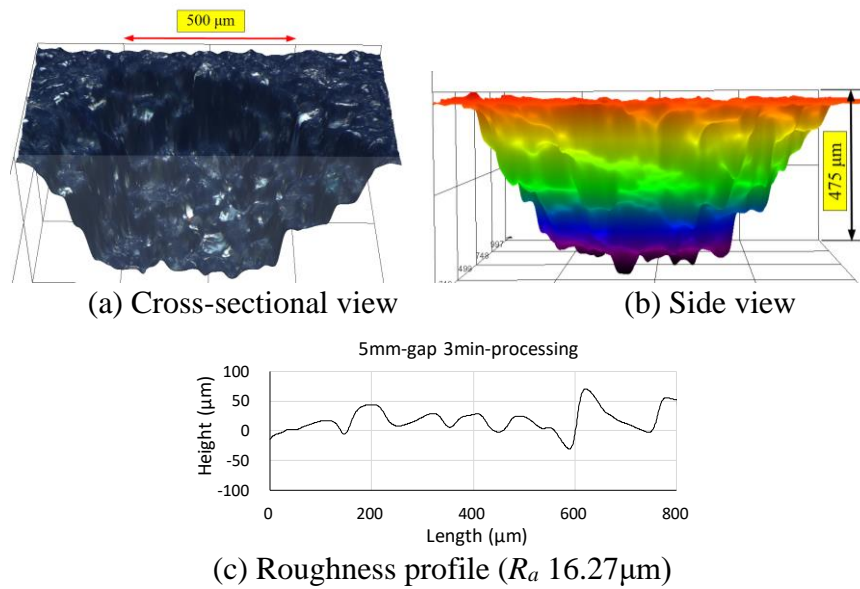

(c) Roughness profile (R_a 16.27μm)

Figure 14. Machined results due to AECJM at 5mm gap and 3 min processing time

It can be seen the surface topography, roughness and geometric shape due to AECJM are very similar to that due to ECJM. Many craters, formed because of SiC particles pull out, can be found at both bottom and sidewall of these machined holes.

3.2.2 Comparison between AECJM and ECJM at 2mm machining gap

Fig. 15 shows comparison of entry diameter, depth, removed volume and machined current between AECJM and ECJM using 2mm gap distance. The results indicate that, for the geometric features, the AECJM generally achieved blind holes with larger entry diameter and smaller depth than the performance of ECJM, as demonstrated in Fig. 15 (a) and (b). Besides, the AECJM also achieved a significant higher material removal rate than the ECJM, as illustrated in Fig. 15(c). This reveals that the holes due to AECJM have a wider open mouth, narrower depth and greater volume than that resulted from ECJM. This phenomenon is relevant to the mechanism of removing SiC$_p$/Al using AECJM at a relatively small gap distance (e.g. 2 mm).

(a)   (b)

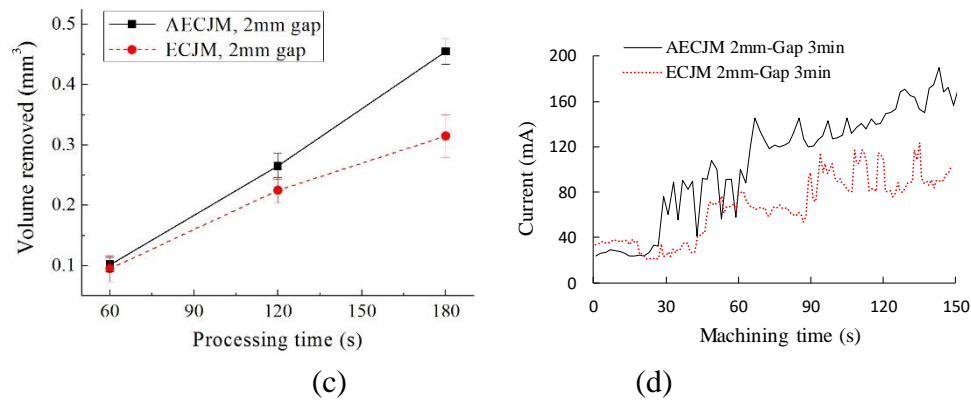(c)   (d)
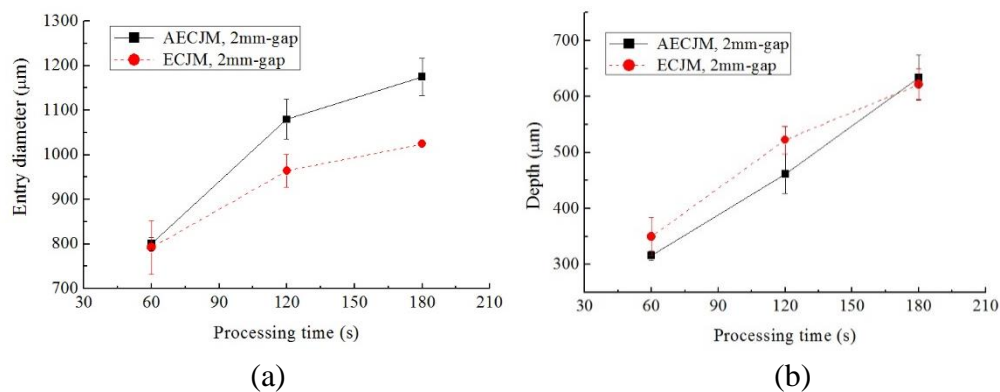
Figure 15. Comparison of machining results at 2mm gap between AECJM and ECJM: (a) entry
diameter, (b) depth, (c) removed volume, and (d) typical machining current

At first, the AECJM can remove aluminum matrix faster than ECJM. As discussed in section
3.1.2, the product of aluminum dissolution at corrosive environment of a neutral electrolyte may involve
a very thin oxide film adjacent to the metal surface which can be continuously removed by electrolyte
flow. With the presence of abrasives, the mixed jet can remove this oxide film faster than pure electrolyte
jet, and consequently results in a higher material removal rate than ECJM. Many authors reported similar
findings regarding this issue. As explained by Wood [20], impinging particles are capable of removing
protective layer on the metal surface and leading to a continuous exposure of fresh metal to the corrosive
environment, and consequently higher current density and corrosion rates. Liu et al. [12] also revealed
this phenomenon through a research of machining micro-channels using AECJM. Another proof of this
point is the machining current measured and demonstrated in Fig. 15(d), wherein the averaged corrosion
current of AECJM is approximate 62% higher than ECJM. Similar to the ECJM, the current due to
AECJM also shows a number of pulsed jump due to SiC particles pull out.

Secondly, relatively higher removal rate of matrix will lead to faster shrinkage of the interface
area between reinforcement and matrix, and subsequently result in faster removal of SiC particles. For
the machining at 2mm gap, the abrasives reach to the target with a relatively low velocity than machining
at larger gap distance. As shown in Fig. 16, Leu et al. [21] and Li et al. [22] divided the structure of a
free water jet in air into three regions, i.e. the initial region, the main region and the diffused droplet
region. Accordingly, Nouraei et al. [23] estimated the abrasive velocity at the centerline, and found that
the centerline abrasives accelerate rapidly within the orifice and for a short distance after they exit,
reaching their maximum velocity after approximately 10 mm where it reach the water velocity. This
indicates that, compared to distance from orifice at 5-10 mm, the impinge kinetic energy of an abrasive
(i.e. $mv^2/2$, where m is mass and v is the velocity of the abrasive) at distance of 2 mm is relative small.
As a result, the number of SiC particles removed from the sidewall due to return abrasive jet flush is
probably greater than that removed from the bottom due to vertical impact of abrasive jet. This caused
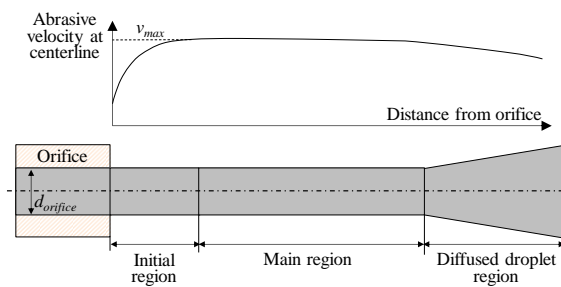wider entry and narrower depth of the holes compared to pure ECJM.

Figure 16. Hypothesized structure of free abrasive electrolyte jet flow in air (not to scale)

3.2.3 Comparison between AECJM and ECJM at 5mm machining gap

Fig. 17 shows comparison of machining performance between AECJM and ECJM using 5mm gap distance. Unlike the machining of 2mm gap, the entry diameter, depth, removed volume and machining current of AECJM are all greater than results of ECJM under comparable conditions. This is consistent with the explanation in section 3.3.2 regarding the abrasive velocity estimated as Fig. 16. According to the correspondent research, the abrasive velocity at the centerline of the jet will reach to a higher speed at 5 mm from orifice exit than at 2 mm from that. As a result, the impinging kinetic energy of abrasives at target distance of 5 mm will be higher than that of 2 mm. This can result in an increase of material removal rate for both reinforcement and matrix, at both positions of bottom and sidewall. The machining current, as shown in Fig. 17(d), also indicates that electrochemical reaction of AECJM is much more intensive than ECJM at a machining gap of 5 mm. However, compared to machining at 2 mm gap, the material removal rate of AECJM at 5mm gap decreases approximate 60 to 70%. In other words, the effect of increasing impinging kinetic energy of abrasives through increasing gap distance cannot compensate the efficacy loss of corrosion rate for aluminum matrix.
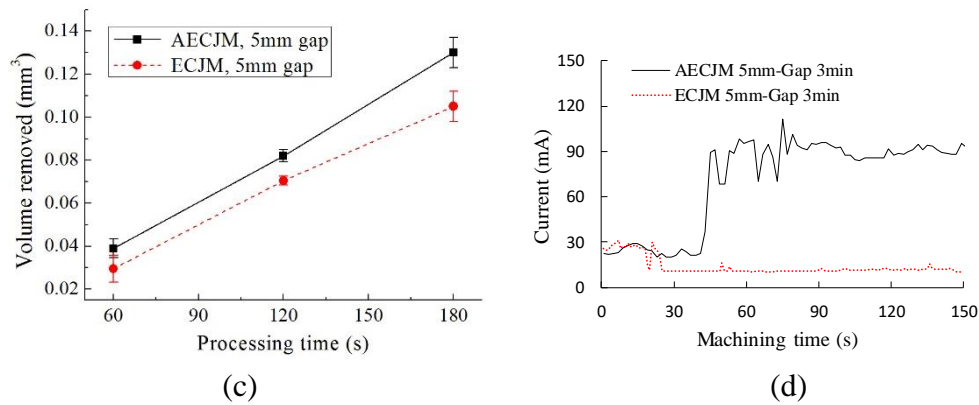

(a)   (b)
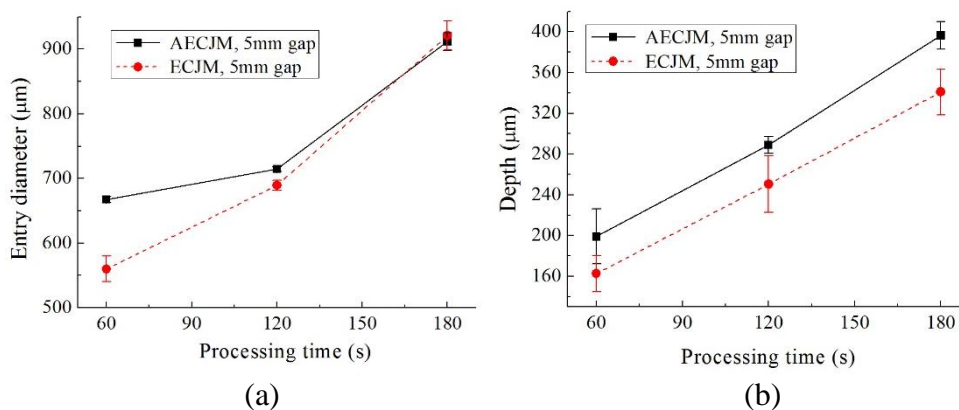
Figure 17. Comparison of machining results at 5mm gap between AECJM and ECJM: (a) entry diameter, (b) depth, (c) removed volume, and (d) typical machining current

4. CONCLUSIONS

The processing of 65%-SiC_p/Al composite using electrochemical jet machining at absence of and presence of abrasive assistance have been investigated. The material removal mechanisms of these processes have been analyzed, and it was found that the removal rate of aluminum matrix determines the removal rate of the composite. Conclusions are summarized as bellow.

Removal mechanism of SiC_p/Al composite using ECJM includes: (i) the aluminum matrix can be removed by electrochemical dissolution, in which the maximum dissolution rate takes place originally along the interface because of high electric field intensity; (ii) the interface can be reduced with the dissolution of matrix, and the maximum dissolution rate moves to the center area between SiC particles because electric field intensity is changed due to continuous protrusion of SiC particles; (iii) the SiC particle will be pulled out from the matrix through jet flushing, when the interface is reduced to a small area.

Compared to the ECJM, the AECJM has a similar removal mechanism and a relatively higher removal rate. This is because high speed impinging abrasives can remove the oxide layer generated at the interface of aluminum and electrolyte. This effect will enhance the corrosion rate of matrix and subsequently result in a faster removal of SiC particles. In general, the entry diameter due to AECJM is larger than that due to ECJM. The machining depth of AECJM can be either smaller or greater than ECJM, in correlation with the target distance.

The machined surface roughness of ECJM and AECJM are significantly affected by the size and fraction of the reinforced particles in the composite. Bigger size of SiC particle will result in larger size of crater due to pull out of the particles, and higher content of reinforcement will lead to a greater number of craters at the machined surface. The result shows that the surface roughness due to AECJM and ECJM at present conditions ranges between R_a 10-16 μm.

Reference

1. P. S. Bains, S. S. Sidhu, H. S. Payal, *J. Mater. Manuf. Process*, 31(2016) 553.
2. C. J. Nicholls, B. Boswell, I. J. Davies, M. N. Islam, *Int. J. Adv. Manuf. Tech*., 90 (2017) 2429.
3. S. T. Huang, L. Guo, H. C. Yang, Y. Su, L. F. Xu, *Int. J. Adv. Manuf. Tech*., 102(2019) 3563.
4. F. Müller, J. Monaghan, *Int. J. Mach. Tool Manu*., 40(2000) 1351.
5. A. Pramanik, *Int. J. Mach. Tool Manu*., 86 (2014) 44.
6. K. K. Saxena, J. Qian, D. A. Reynaerts, *Int. J. Mach. Tool. Manuf*., 127(2018) 28.
7. M. Hackert-Oschätzchen, G. Meichsner, M. Zinecker, André Martin, A. Schubert, *J. Precis. Eng*., 36(2012) 612.
8. I. Bisterov, J. Mitchell-Smith, A. Speidel, A. Clare, *Procedia Cirp*, 68(2018) 460.
9. J. Mitchell-Smith, A. Speidel, J. Gaskell, A. T. Clare, *J. Int. J. Mach. Tool. Manuf*., 122(2017) 32.
10. N. Lehnert, N. Hackert-Oschätzchen, A. Martin, A. Schubert, *Procedia Cirp*, 68(2018)471.
11. Z. Liu, H. Nouraei, M. Papini, J. K. Spelt, *J. Mater. Process. Tech*, 214 (2014) 1886.
12. Z. Liu, C. S. Gao, K. Zao, K. Wang, *Int. J. Adv. Manuf. Tech*, 95(2018) 1143.
13. T. F. Che, L.Y. Long, Y. J. Chun, *Ind. Lubr. Tribol.,* 70(2018) 1545.
14. M. M. Lohrengel, K. P. Rataj, T. Münninghoff, *J. Electrochim. Acta*, 201(2016) 348.
15. J. Ano, A. S. Assémian, Y. A. Yobouet, K. Adouby, P. Drogui, *J. Process Saf. Environ. Prot*., 129(2019) 184.
16. M. Hackert-Oschätzchen, R. Paul, A. Martin, G. Meichsner, N. Lehnert, A. Schubert, *J. Mater. Process. Tech*., 223(2015) 240.
17. T. Haisch, E. Mittemeijer, J. W. Schultze, *Electrochimica Acta*, 47(2001) 235.
18. A. C. West, C. Madore, C. Matlosz, D. Landolt, *J. Electrochem. Soc*., 139(1992), 499.
19. T. Baldhoff, V. Nock, A. T. Marshall, *J. Electrochem. Soc.*, 165(2018) 841.
20. R. J. K. Wood, *Wear,* 261(2006) 1012.
21. M. C. Leu, P. Meng, E. S. Geskin, et al., *J. Manuf. Sci. Eng.,* 120(1998) 571.
22. H. Z. Li, J. Wang, J. M. Fan, *Int. J. Mach. Tool. Manuf*., 49(2009) 850.
23. H. Nouraei, A. Wodoslawsky, M. Papini, J. K. Spelt, *J. Mater. Process. Tech*., 213(2013)1711.